

Spectroscopic, Electroanalytical, and Hydrolytic-Like Activities of Bis(2-picolyl)Glycine-Based Zinc(II) and Copper(II) Complexes

Mohamed M. Ibrahim^{1,2,*} and Gaber A. M. Mersal^{2,3}

¹Chemistry Department, Faculty of Science, Kafr El-Sheikh University, Kafr El-Sheikh, Egypt

²Department of Chemistry, Faculty of Science, South Valley University, Qena, Egypt

³Chemistry Department, Faculty of Science, Taif University, Taif, Saudi Arabia

*E-mail: ibrahim652001@yahoo.com

Received: 9 November 2012 / Accepted: 12 December 2012 / Published: 1 January 2013

Complex formation of the tetradentate ligand bis(2-picolyl)glycine, BPG, with both Zn(II) and Cu(II) ions in aqueous solution was investigated spectroscopically by using ¹H NMR and UV-visible titrations as well as electrochemically by using cyclic voltammetry. Analysis of the titration data indicated that the aqua complexes [BPG-Zn(OH₂)₂]⁺ **1** and [BPG-Cu(OH₂)₂]⁺ **2** deprotonate at pH = 10.6 and 9.7. The catalytic hydrolysis of the activated phosphate ester tris(*p*-nitrophenyl) phosphate (TNPP) by using these model complexes was examined and the released phenolate anions were determined by using electroanalytical technique. The kinetic results indicate that copper(II) complex **2** is more active hydrolytic catalyst than zinc(II) complex **1**, presumably a reflection of the effective electron-withdrawing as well as the greatest electrophilicity of copper(II) ion.

Keywords: Pyridine-containing ligand; Electroanalytical; ¹H NMR titration; Phosphate ester hydrolysis.

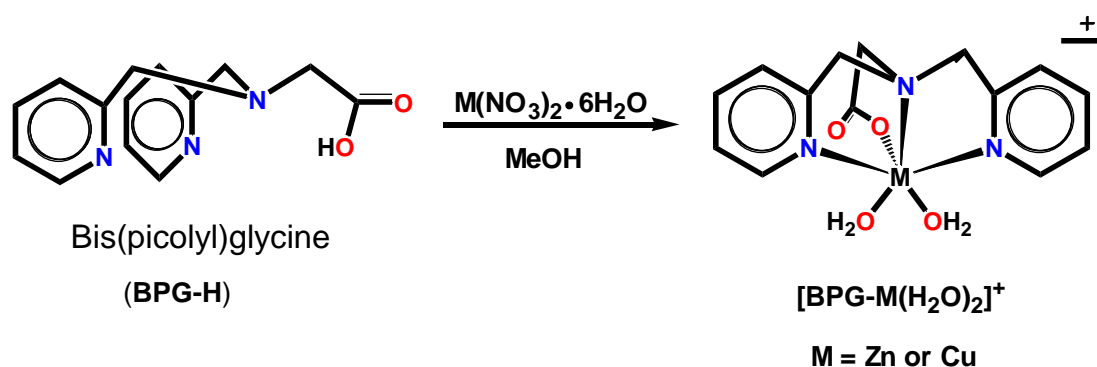
1. INTRODUCTION

Insecticides are important environmental pollutants. The continuous increase in agricultural production promotes an equivalent increase in the level of insecticide residues in water, soil land foodstuff. Prevention of the negative effects of the insecticides requires a systematic control of the content of their remains in agricultural products, food, soil, and water. Therefore, the determination of *p*-nitrophenol in these environmental samples is very important due to their toxic effects. The source of *p*-nitrophenols in environment comes as a product from degradation of several organophosphorous pesticides such as fenitronthion and parathion. Different analytical techniques were used for

monitoring of *p*-nitrophenolate in different fields, these techniques includes gas and liquid chromatography (HPLC) [1-5] and spectroscopic methods [6-9]. Electrochemical methods were also used for the determination of *p*-nirtopheol such as anodic stripping voltammetry, differential pulse polarography and differential pulse voltammetry [10-14].

Recently there has been growing interest in the metal ion-promoted hydrolysis of phosphate esters as model systems for *metallophosphatase* enzymes as well as potential catalysts for the detoxification of *anticholinesterase* agents used in chemical warfare [15-17]. Among the hydrolytic metalloenzymes the (N,N,O)Zn–OH₂ donor motif (with N representing histidine and O representing aspartate or glutamate) is a very common one [18,19] being present for instance in two of the best known enzymes, *carboxypeptidase* and *phosphotriestrase* [20]. Accordingly, the challenge of modeling such enzymes with coordination compounds of zinc calls for the design and synthesis of polydentate ligands with uncharged nitrogen and anionic oxygen donors [21-24].

As a part of our studies in the biomimetic hydrolytic metalloenzymes [25-39] and with the aim to mimic the key features of these metalloenzymes, the synthesized diaqua complexes of both zinc(II) and copper(II) [BPG-M(OH₂)₂] {BPG = *N,N*-bis(2-picolyl)glycine, BPG-H & M²⁺ = Zn²⁺ **1** and M²⁺ = Cu²⁺ **2**} (Scheme 1) as and functional models for the active site of *hydrolase* enzyme towards the hydrolysis of phosphate esters. These complexes were structurally analyzed in solution by means of cyclic voltammetry and ¹H NMR spectroscopy. The catalytic activity of these model complexes as potential catalysts toward the hydrolysis of the activated phosphate triester tris(*p*-nitrophenyl)phosphate TNPP, which mimic the toxic organophosphorous pesticides such as parathion and paraoxon was also examined using spectroscopic and electroanalytical techniques.



Scheme 1. The structure of the ligand bis(picolyl)glycine (BPG-H) and its zinc(II) and copper(II) complex species.

2. EXPERIMENTAL

2.1. General details

All reagents were commercial grade materials and were used without further purification. All solvents were dried and distilled by standard methods. The IR absorption spectra were recorded using FT-IR Prestige-21 Shimadzu, in the range of 400- 4000 cm⁻¹. ¹H NMR spectra were measured on a JEOL EX-400 instrument. UV–visible absorption spectra were recorded on a UV-1650

spectrophotometer SHIMADZU using a tandem cuvette at 25 °C. The electrical conductivity measurements at room temperature were carried out using Equiptronics digital conductivity meter model JENWAY 4070 for (1×10^{-3} M) solutions. The synthesis of the ligand bis(2-picolyl)glycine, BPG and its zinc(II) and copper(II) complexes were carried as previously established method [32].

2.2. Cyclic voltammetry

The electrochemical behavior of the tetradentate ligand L and its zinc(II), copper(II) complexes was studied using cyclic voltammetry (CV) and square wave voltammetry (SWV) using auto lab potentiostat PGSTAT 302 (Eco Chemie, Utrecht, The Netherlands) driven by the General Purpose Electrochemical Systems data processing software (GPES, software version 4.9, Eco Chemie). The electrochemical cell used in this work contains three electrodes; platinum wire was used as a working electrode, SCE as a reference electrode, and a platinum wire was used as a counter electrode.

2.3. Zinc(II) titration by using ^1H NMR measurements

To investigate the coordination behavior toward zinc ions, ^1H NMR analyses of the nature of BPG / Zn^{2+} binding in D_2O and $I = 0.1$ M NaNO_3 were undertaken as a function of pD and at different zinc-to-ligand ratios. The chemical shifts are reported relative to the resonance signal of sodium 2,2-dimethyl-2-silapentane-5-sulfonate (DSS) as an internal standard signals. The pD was adjusted with concentrated NaOD and DNO_3 , so that the effect of dilution could be neglected.

2.5. Computational studies

Molecular modeling and quantum semi – empirical calculations were carried out using ZINDO/1 method of Hyperchem 7.5 software from Hypercube. The geometry optimizations of the ligand and their metal copper complexes were obtained by the application of the Polak–Ribiere algorithm with convergence limit of 0.01 kcal/mol and RMS gradient of 0.01 kcal / mol.

3. RESULTS AND DISCUSSION

3.1. Electrochemical studies of the Ligand L and its zinc(II) and copper(II) complexes

The electrochemical behavior of the ligand and its zinc(II) and copper(II) complexes **1** and **2** were studied using cyclic voltammetric techniques. The cyclic voltammetry was carried out in 10 mL electrochemical cell containing 0.1 M of $[\text{NBu}_4][\text{ClO}_4]$ in DCM in a potential range from -1.5 to + 2.0 V (vs. SCE) and scan rate of 100 mVs^{-1} . No peaks appeared under the studied conditions in the absence of the ligand BPG-H. In the presence of 1 mM of L (Figure 1), two quasi-reversible redox couple waves were observed: two anodic peaks at -0.17 V (Epa1) and 1.66 V (Epa2) in the forward

scan and another two cathodic peaks at -0.55 V (Epc1) and 0.84 V (Epc2) in the reverse scan. The peak separation potential $\Delta E = (E_{pa} - E_{pc})$, between the first couple (Epa1 and Epc1) and second couple (Epa2 and Epc2) are 380 mV and 820 mV, respectively. These large peak separation potentials suggest a quasi-reversible behavior. The appearance of the first couple might be due to one electron oxidation of the ligand, while the second couple might be due to the oxidation process carboxylic group of L. The electrochemical behavior of zinc (II) and copper(II) complexes was also investigated under the same conditions. In the case of zinc(II) complex (Figure 2a) for the first couple peaks, the oxidation peak shifted to more positive value (Epa1 = 0.27) and the reduction peak (Epc1) shifted to more positive value (+ 0.53 V vs. SCE). In the second redox couple, the oxidation peak shifted to more negative value (Epa2 = + 1.57 V vs. SCE) and the cathodic peak shifted to more positive value (Epc2 = + 0.93 V vs. SCE). Also one quasi-reversible redox waves appeared at (Epa3 = 0.04 V and Epc3 = - 0.1V vs. SCE) was observed. The peak separation potential $\Delta E = (E_{pa3} - E_{pc3})$ is 60 mV. This might be due to one electron redox process for Zn^{2+}/Zn^{+1} .

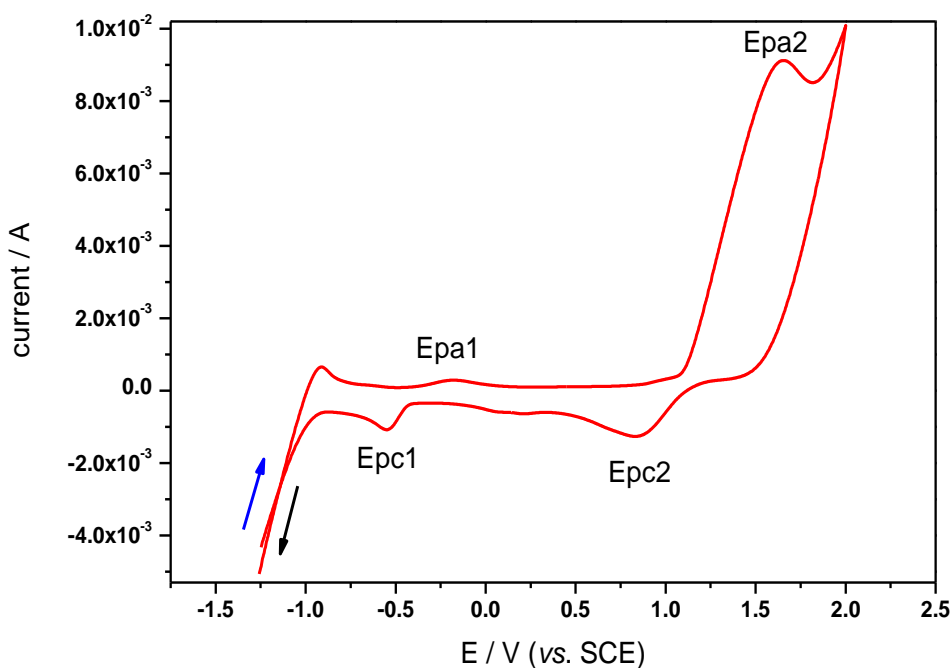


Figure 1. Cyclic voltammogram for 1 mM BPG-H in DCM containing 0.1 M $[NBu_4][ClO_4]$ as a supporting electrolyte using scan rate 100 mV/s.

The same behavior was observed for the case of copper (II) complex. The resulting voltammogram (Figure 2b), the two quasi-reversible couples electron redox couples peaks were shifted.

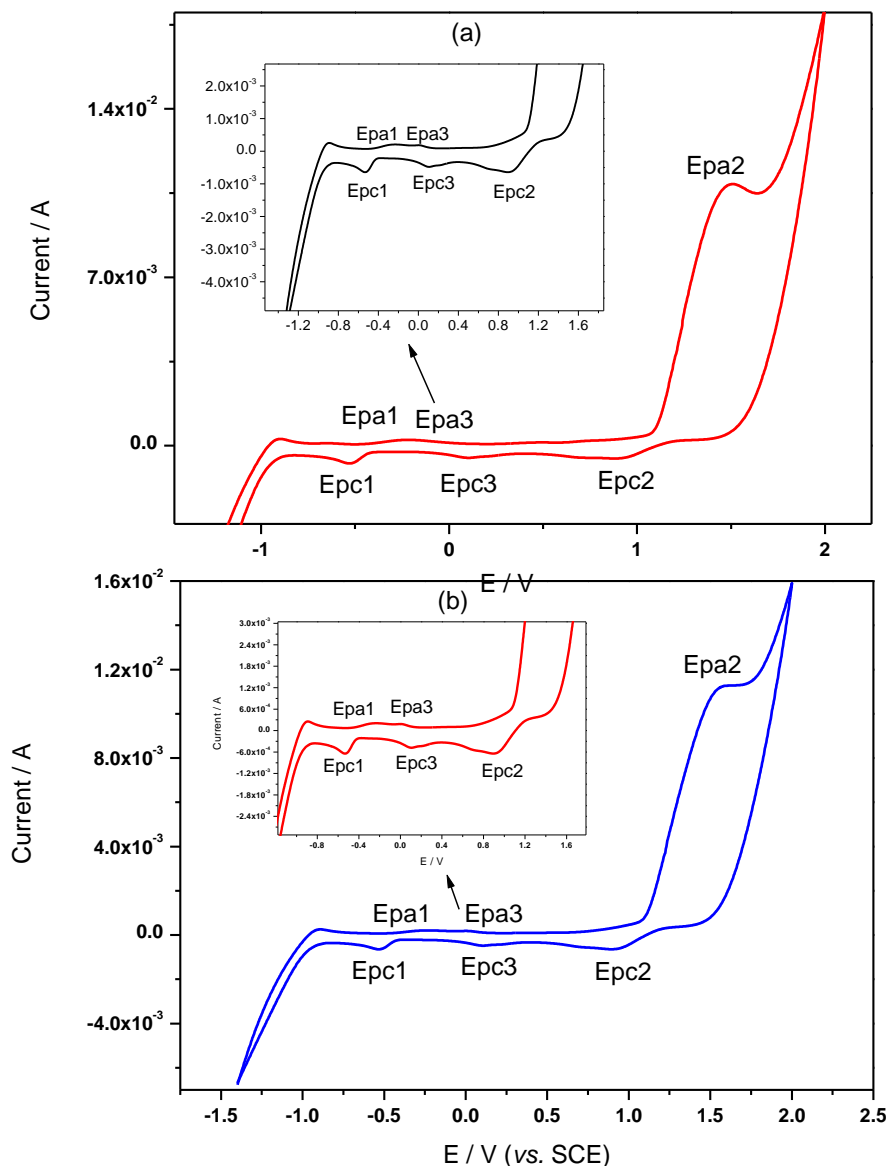


Figure 2. Cyclic voltammograms for (a) [BPG-Cu(H₂O)₂](NO₃) **2** and (b) [BPG-Zn(H₂O)₂](NO₃) **1**. Conditions as mentioned.

For the first couple peaks, the oxidation peak shifted to more positive value (Epa1 = 0.23) and the reduction peak (Epc1) shifted to more positive value (+ 0.53 V vs. SCE). In the second redox couple, the oxidation peak shifted to more negative value (Epa2 = + 1.5 V vs. SCE) and the cathodic peak shifted to more positive value (Epc2 = + 0.9 V vs. SCE). Also for copper (II) complex another one reversible redox waves (Epa3 = -0.16 V and Epc3 = -0.1V vs. SCE) was observed. The peak separation potential $\Delta E = (E_{pa3} - E_{pc3})$ is 60 mV. This reversible redox waves might be due to one electron redox process for Cu²⁺/Cu⁺¹ [40].

3.2. Zinc(II) titration

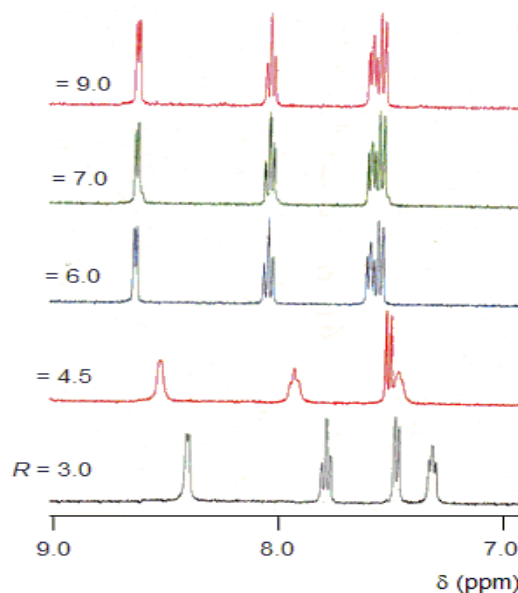


Figure 3. ^1H NMR spectra of the aromatic regions of the ligand BPG (2.0×10^{-3} M) as a function of Zn^{2+} at different ratios ($R=[\text{Zn}^{2+}]/[\text{BPG}]$, 0.0-2.0) at a pD = 8.5 in D_2O ($I = 0.1$ M NaNO_3 , 25 ± 0.1 °C).

The stoichiometry of zinc(II) complex **1** was determined by recording the chemical shifts of the pyridine protons and methylene protons of the produced zinc(II) complex **1** at different ratios of solutions of the zinc salt and the ligand L in D_2O . Figure 3 showed that with increasing the concentration of zinc(II) ions, there is broadening and downfield shifts of the pyridine protons of the produced zinc(II) complex species between $0 < R < 1$. This finding can be attributed to the exchange interaction between the complex at the molar ratio 1:1 and the free ligand. Further increments of zinc(II) ions does not change the chemical shift, that is why formation of zinc complexes with 1:1 stoichiometry is thought and the composition is $[\text{BPG-Zn}(\text{H}_2\text{O})_2]^+$ **1**, mononuclear model complex.

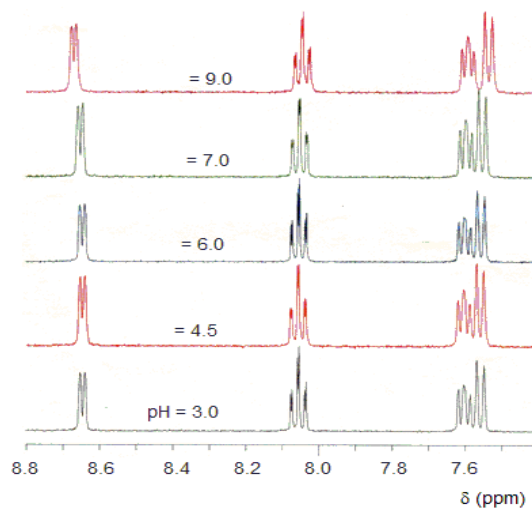


Figure 4. ^1H NMR spectra of the aromatic regions of Zinc(II) complex **1** (2.0×10^{-3} M) as a function of pD = 8.5 in D_2O ($I = 0.1$ M NaNO_3 , 25 ± 0.1 °C).

The observed ^1H NMR signals of the aromatic and aliphatic protons of the zinc compound **1** species at $R = 1$ was shown in figure 3. The chemical shift of these signals were constant between pD 5.9 and 8.9, which means the formation of 1:1 complex species $[\text{BPG-Zn}(\text{OH}_2)_2]^+$. Further upfield chemical shift (Figure 4) indicates deprotonation of the aqua $[\text{BPG-Zn}(\text{OH}_2)_2]^+$ to the hydroxo species $[\text{BPG-Zn}(\text{OH})(\text{OH}_2)]^+$.

The 0.4–0.6 ppm downfield shift for zinc-bound $\text{H}_2\text{O}/\text{OH}$ compared with the chemical shift of the free waters resulted from the decrease in electron density due to the coordination to zinc(II) ion. This is mainly attributed to the effect of Lewis acidity of zinc. The ca. 0.2 ppm upfield shift for zinc-bound OH, compared with the chemical shift of zinc-bound H_2O , resulted from the increase of electron density by the deprotonation of zinc-bound H_2O .

3.3. Computational Studies

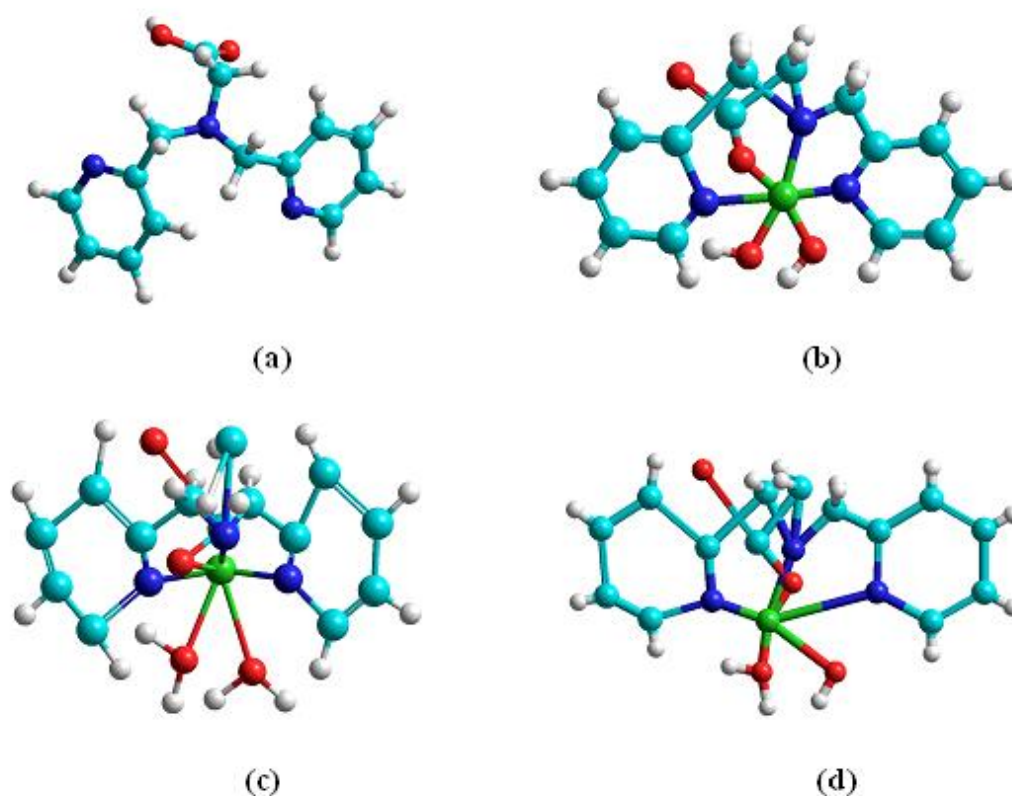


Figure 5. Ball and stick model for the optimized geometries of (a) BPG-H and its copper complexes (b) $[\text{BPG-Cu}(\text{OH})_2]^+$, (c) $[\text{BPG-Cu}(\text{H}_2\text{O})_2]^+$, and (d) $[\text{BPG-Cu}(\text{H}_2\text{O})(\text{OH})]$ obtained from semi-empirical ZINDO/1 method.

Geometry optimization calculations employ energy minimization algorithms to locate stable structures. The optimized structure of the ligand and its copper(II) complexes $[\text{BPG-Cu}(\text{H}_2\text{O})_2]^+$, $[\text{BPG-Cu}(\text{H}_2\text{O})(\text{OH})]$, and $[\text{BPG-Cu}(\text{OH})_2]^+$ obtained through molecular mechanics calculation by applying semi-empirical ZINDO/1 method are shown in Figure 5. Figure 6 shows that the highest

energy occupied orbitals (HOMOs) are mainly localized at the pyridine groups for the ligand molecule BPG-H with energy value of - 7.92 eV.

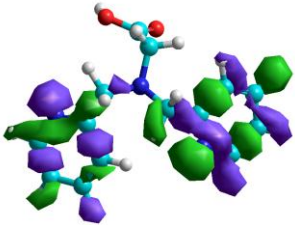
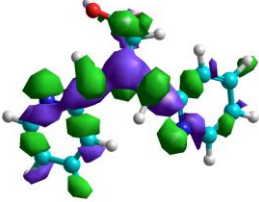
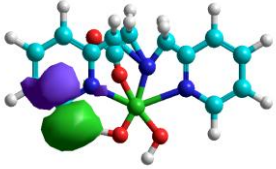
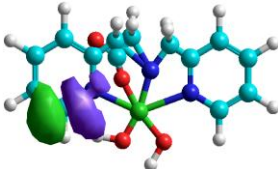
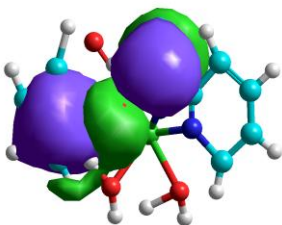
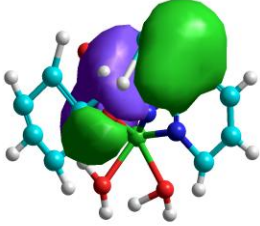
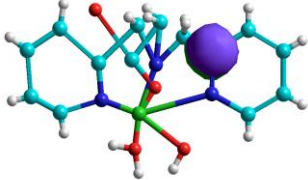
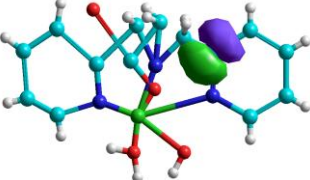
	HOMO	LUMO
BPG-H	 E = -7.92 eV	 E = -7.488 eV
BPG-Cu(OH) ₂	 E = -8.887 eV	 E = -6.192 eV
BPG-Cu(H ₂ O) ₂	 E = -320.4646 eV	 E = -34.5714 eV
BPG(H ₂ O)(OH)	 E = -45.9865 eV	 E = -48.214 eV

Figure 6. HOMO and LUMO orbitals with energy for of BPG-H and its copper and Zinc complexes obtained from semi-empirical ZINDO/1 method.

While for the $[\text{BPG-Cu}(\text{H}_2\text{O})_2]^+$, the HOMO orbitals are localized on the pyridine group, tertiary amine and copper atom with energy value of 32.04646 eV. In the other hand, the HOMO orbitals of $[\text{BPG-Cu}(\text{H}_2\text{O})(\text{OH})]$ are localized on the carbon of one pyridine group with - 45.9864 eV energy. For the case of $[\text{BPG-Cu}(\text{OH})_2]^-$, the HOMO orbitals are localized on the hydroxyl ion OH^- and one carbon of the pyridine group with -8.887 eV energy.

The lowest energy unoccupied orbitals (LUMOs) for the BPG-H ligand are localized at the pyridine group with a contribution of the central tertiary amine and carboxylic group with energy value of - 7.488 eV. The LUMOs orbitals for the $[\text{BPG-Cu}(\text{H}_2\text{O})_2]^+$ are localized on the tertiary amine, pyridine group and partially on copper atom with energy value of - 35.5714eV. The LUMOs orbitals of $[\text{BPG-Cu}(\text{H}_2\text{O})(\text{OH})]$ are localized on the pyridine group with - 48.214 eV energy. Whereas the LUMOs orbitals of $[\text{BPG-Cu}(\text{OH})_2]$ are located on the hydrogen atoms of the pyridine rings and the OH ion with energy value of - 6.192 eV. The value of the energy separation between the HOMOs and LUMOs are 2.695 eV, 2.525 eV and 2.228 eV for the complexes $[\text{BPG-Cu}(\text{OH})_2]^-$, $[\text{BPG-Cu}(\text{H}_2\text{O})(\text{OH})]$, and $[\text{L-Cu}(\text{H}_2\text{O})_2]^+$, respectively. these values are in good in agreement with the value of 2–3 eV, which are often encountered for stable transition metal complexes [41].

3.4. Kinetic Hydrolysis of TNPP

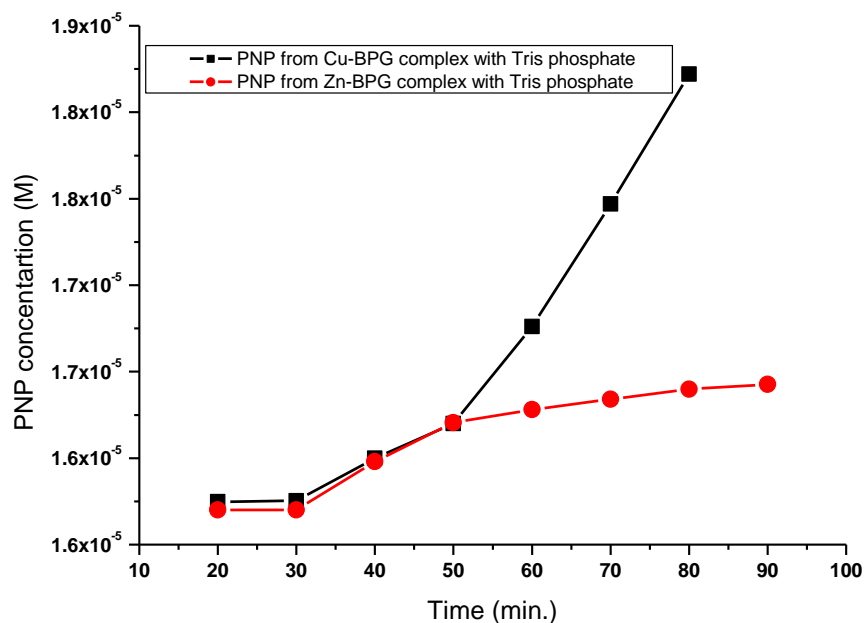
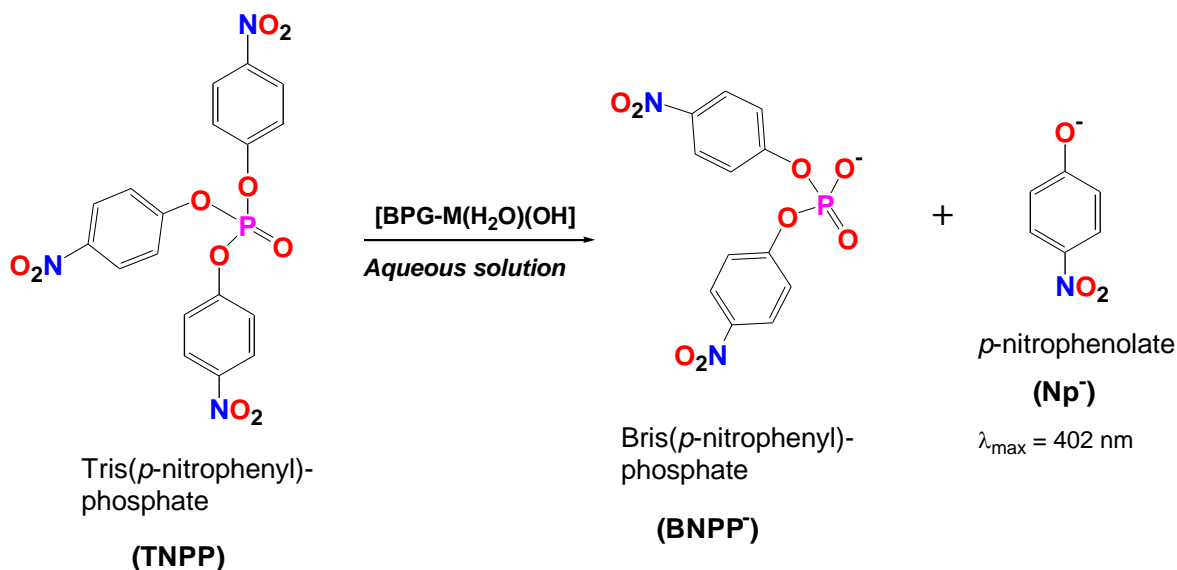


Figure 7. Time course for the released *p*-nitrophenolate obtained from the hydrolysis of *p*-NPDPP catalyzed by using complexes **1** and **2**.

The hydrolysis of tris(*p*-nitrophenyl)phosphate, TNPP has been examined electroanalytically using the model complexes **1** and **2**. Upon hydrolysis, TNPP decompose into *p*-nitrophenolate, (NP^-) and bis(*p*-nitrophenyl)phosphate (BNPP^-), respectively (Scheme 2). The released *p*-nitrophenolate was

determined using square wave voltammetry using screen printed gold electrode as a working electrodes. The catalytic hydrolysis of TNPP by using both complexes **1** and **2** was examined by following the produced amount of *p*-nitrophenol. Figure 7 showed that by increasing the decomposition time, the concentration of the released *p*-nitrophenolate was increased. The rate of the decomposition by using complex **2** was found to be higher than that of complex **1**.



Scheme 2. The hydrolysis reaction of the phosphate triester TNPP by using the model complexes

On the basis of the above mentioned spectroscopic and electroanalytic studies of the triester TNPP in aqueous medium and the isolation of the hydrolyzed product BPGZn(II)-bound bis(*p*-nitrophenyl)phosphate complex [42], we proposed a mechanism for the hydrolysis of TNPP (Scheme 2). At the first step: the coordinated water molecule in both complexes **1** and **2** can deprotonate, producing the metal(II)-bound hydroxo species [5, 6]. Second: the metal center delivers the coordinated hydroxide, which can nucleophilically attack the TNPP molecule, while the metal ion simultaneously withdraw electron density away from the phosphorus atom by interacting with the phosphoryl oxygen, forming pentacoordinated intermediate; finally, the *p*-nitrophenolate is released and the metal(II)-bound bis(*p*-nitrophenyl) phosphate [5], which could be isolated from methanolic solution is replaced by water to form again the starting catalyst aqua metal(II) complexes, which are ready to start another catalytic cycle.

4. CONCLUSION

Solution studies of the metal-ligand interactions were carried out for determining the stoichiometry and the pK_a value of the coordinated water molecules using ^1H NMR and UV-visible spectrosopes. The reactivity of these aqua model complexes as potential catalysts, for the hydrolysis

of the trimester, tris(*p*-nitrophenyl)phosphate, *TNPP* has been investigated. The reported catalytic studies demonstrated that the reactivity of the investigated complexes show dependency on the nature of the metal ions. The results of the catalytic investigations showed that the copper(II) complexes [BPG-Cu(H₂O)₂]⁺ **2** is more effective hydrolytic catalyst than the zinc(II) analogues **1**.

References

1. K.C. Honeychurch, J.P. Hart, *Electroanalysis* 19, 2176 (2007).
2. R. Belloli, B. Barletta, E. Bolzacchini, S. Meinardi, M. Orlandi, B. Rindone, *J. Chromatogr. A* 846, 277 (1999).
3. H. B. Böhm, J. Feltes, D. Volmer, K. Levsen, *J. Chromatogr.* 478, 399 (1989).
4. A. Brega, P. Prandini, C. Amaglio, E. Pafumi, *J. Chromatogr. A* 535, 311 (1990).
5. J. J. Scanlon, P.A. Falquer, G.W. Robinson, G.E. Brien, P.E. Sturrock, *Anal. Chim. Acta* 158, 169 (1984).
6. Q. Zhou, Y. Xi, H. He, R.L. Frost, *Spectrochim. Acta A: Mol. Biomol. Spectrosc.* 69, 835 (2008).
7. M. Tian, L. Bakovic, A. Chen, *Electrochim. Acta* 52, 6517 (2007).
8. Q. Zhou, Y. Xi, H. He, R.L. Frost, *Spectrochim. Acta A: Mol. Biomol. Spectrosc.* 69, 835 (2008).
9. X. Zhu, S. Shi, J. Wei, F. Lv, H. Zhao, J. Kong, Q. He, J. Ni, *Environ. Sci. Technol.* 41, 6541 (2007).
10. I.N. Rodri'guez, J.A.M. Leyva, J. Hidalgo, H. de Cisneros, *Anal. Chim. Acta* 344, 167–173 (1997).
11. J. Fischer, L. Vanourkova, A. Danhel, V. Vyskocil, K. Cizek, J. Barek, K. Peckova, B. Yosypchuk, T. Navratil, *Int. J. Electrochem. Sci.* 2, 226 (2007).
12. P. Mulchandani, C.M. Hangarter, Y. Lei, W. Chen, A. Mulchandani, *Biosens. Bioelectron* 21, 523 (2005).
13. R.d.S. Luz, F.S. Damos, A.B. de Oliveira, J. Beck, L.T. Kubota, *Talanta* 64, 935 (2004).
14. S. Hu, C. Xu, G. Wang, D. Cui, *Talanta* 54, 115 (2001).
15. R. H. Hay, Reactions of Coordinated ligands (Edited by P. S. Bratermen) Vol. 2, p. 316. Plenum, New York (1989).
16. R. W. Hay, Comprehensive Coordination Chemistry (Edited by G. Wilkinson, R. D. Gillard and J. A. McCleverty), Vol. 6, p. 411. Pergamon Press, Oxford (1987).
17. R. Morrow, W.C. Trogler, *Inorg. Chem.* 28 (1989) 2330; (c) R. Hendry, A.M. Sargeson, *J. Am. Chem. Soc.* 111 (1989) 2521.
18. T. G. Spiro (Ed.), Zinc Enzymes, Wiley, New York (1983).
19. H. Sigel (Ed.), Metal ions in biological systems, Zinc and its Role in Biology and Nutrition, vol. 15, Marcel Dekker, New York (1979).
20. D. W. Christianson, W. N. Lipscomb, *Acc. Chem. Res.*, 22 (1989) 62.
21. S. S. Tandon, S. Chander, L. K. Thompson, J. N. Bridson, V. McKee, *Inorg. Chim. Acta*, 219 (1994) 55.
22. J. T. Groves, J. R. Olson, *Inorg. Chem.*, 24 (1985) 2717.
23. A. Schepartz, R. J. Breslow, *J. Am. Chem. Soc.*, 109 (1987) 1814.
24. A. Abufarang, H. Vahrenkamp, *Inorg. Chem.*, 34 (1995) 3279.
25. M. M. Ibrahim, K. Ichikawa, M. Shiro, *Inorg. Chem. Commun.*, 6 (2003) 1030.
26. M. M. Ibrahim, K. Ichikawa, M. Shiro, *Inorg. Chim. Acta*, 353 (2003) 187.
27. T. Echizen, M. M. Ibrahim, K. Nakata, M. Izumi, K. Ichikawa, M. Shiro, *J. Inorg. Biochem.*, 98 (2004) 1347.
28. M. M. Ibrahim, *Inorg. Chem. Commun.*, 9 (2006) 1215.
29. M. M. Ibrahim, S. Y. Shaban, K. Ichikawa, *Tetrahedron Letters*, 49 (2008) 7303.
30. M. M. Ibrahim, G. M. Mersal, *J. Inorg. Organomet. Polym.* 19 (2009) 549.

31. M. M. Ibrahim, A. M. Ramadan, *J. Incl. Phenom. Macrocycl. Chem.* 72 (2012) 103-111.
32. M. M. Ibrahim, *J. Mol. Struct.* 990 (2011) 227-236.
33. M. M. Ibrahim, G. A. M. Mersal, *J. Inorg. Biochem.* 104 (2010) 1195-1204.
34. M. M. Ibrahim, M. A. Ramadan, *J. Incl. Phenom. Macrocycl. Chem.* 68 (2010) 287-296.
35. M. M. Ibrahim, H. A. Eissa, G. E. Kamel, and H. Y. El-Baradie, *Synthesis and Reactivity in Inorganic, Metal-Organic, and Nano-Metal Chemistry.* 40 (2010) 869-878.
36. M. M. Ibrahim, M. Shu, H. Vahrenkamp, *Eur. J. Inorg. Chem.* (2005) 1388.
37. M. M. Ibrahim, N. Shimomura, K. Ichikawa, M. Shiro, *Inorg. Chim. Acta*, 313 (2001) 125.
38. M. M. Ibrahim, *J. Inorg. Organomet. Polym.*, 19 (2009) 532.
39. M. M. Ibrahim, M. A. Amin, K. Ichikawa *J. Mol. Struct.* 985 (2011) 191-201.
40. S. S. Shammi, A. A. Shaikh, S. M. S. Islam, M. Q. Ehsan, *Malays. J. Chem.* 10 (2009) 9.
41. P. J. Blower, J. R. Dilworth, R. I. Maurer, G. D. Mullen, C. A. Reynolds, Y. Zheng, *J. Inorg. Biochem.* 85 (2001) 15.
42. A. Abufrag, H. Vahrenkamp, *Inorg. Chem.* 34 (1995) 2207.